In-vivo distributed multicellular control of gene expression in microbial consortia

Davide Salzano[a,b], Barbara Shannon[b], Claire Grierson[c,d],
Lucia Marucci[d,e,f*], Nigel J Savery[b,d*], Mario di Bernardo [a,g,*]

[a]*Scuola Superiore Meridionale, Naples, Italy*

[b] *School of Biochemistry, University of Bristol, United Kingdom*

[c] *School of Biological Sciences, University of Bristol, United Kingdom*

[d] *Bristol BioDesign Institute, University of Bristol, United Kingdom*

[e] *School of Engineering Mathematics and Technology, University of Bristol, United Kingdom*

[f] *School of Cellular and Molecular Medicine, University of Bristol, United Kingdom*

[g] *Department of Electrical Engineering and Information Technology, University of Naples Federico II, Italy*

* *These authors contributed equally*

[#] Correspondence should be addressed to: mario.di.bernardo@unina.it

Keywords: Cybergenetics, synthetic biology, control engineering, multicellular control, microbial consortia, gene regulation, Escherichia coli, modularity, biomedicine, industrial bioproduction.

Abstract

This paper presents an innovative approach in synthetic biology, focusing on the engineering of biomolecular feedback control systems within microbial consortia to achieve robust and precise regulation of desired phenotypes. Traditional biomolecular control strategies, while effective, are predominantly confined to single-cell applications, limiting their complexity and adaptability due to metabolic constraints. We propose a novel methodology that distributes control functionalities across different cell populations within a microbial consortium. This approach leverages the division of labor and cooperative interactions among microbial populations, significantly enhancing flexibility and robustness. We build on the foundation of synthetically engineered microbial consortia, known for their applications in complex compound production and advanced computational processes. However, the challenge of implementing a distributed feedback control loop for precise phenotype regulation in synthetic communities has remained unaddressed. Our work closes this gap by developing and validating an in-vivo feedback control loop distributed across a bacterial consortium, specifically designed using two Escherichia coli strains. These strains are engineered to perform the three essential control functions: computation, sensing, and actuation. We employ orthogonal quorum sensing signaling molecules for communication between the controller and target cell populations. Through in-vivo experiments, we compare closed-loop and open-loop configurations to demonstrate the effectiveness of our approach. The results show that our distributed control system can regulate gene expression levels in target populations with high precision and robustness, even in the presence of consortium composition variations. This feature is particularly vital for practical applications in synthetic biology where stability and adaptability are crucial. Our study not only addresses a significant gap in synthetic biology literature but also opens avenues for more complex and reliable synthetic biology applications.

Introduction

Synthetic biology aims to engineer biomolecular systems to achieve new functions [1]; potential applications range from designing bacteria that can produce biofuels or sense and degrade pollutants in the environment (such as hydrocarbons and plastics), to immune cells

that can track and kill cancer cells, or that can release drugs at specific points in desired conditions to avoid side effects (see [2] for an extensive review). Biomolecular feedback controllers have been highlighted as a crucial ingredient for reliable and robust synthetic biology devices, increasing their flexibility and modularity [3]–[5].

Different designs have been proposed to implement biomolecular feedback control strategies both in-silico and in-vivo, ranging from simple feedback and feedforward loops to PID (Proportional Integral Derivative) controllers (see [3] and references therein). In particular, the introduction of an integral control action via an antithetic feedback motif has been highlighted as a fundamental ingredient for a synthetic circuit able to achieve and maintain a desired output even in the presence of disturbances, a property that has been termed *robust perfect adaptation* [6]. Integral biomolecular controllers have been thoroughly studied both theoretically [7]–[9] and experimentally, and different implementations have been proposed in bacteria [10] and mammalian cells [11]. For a review of the recent advancements in the implementations of biomolecular controllers guaranteeing robust perfect adaptation see [4].

However, existing robust controllers predominantly function at the single-cell level, posing inherent limitations on circuit complexity due to metabolic burden, and hindering their application as flexible plug-and-play modules across diverse synthetic and endogenous systems [5]. To overcome these constraints, following [12], we propose to distribute the required functionalities across distinct cell populations within a microbial consortium. Each cell strain encapsulates specific engineered gene networks, forming the foundation for a distributed feedback control loop [13], [14] involving two populations: a controller population and a target cell population. The former senses the targets' output, compares it with a reference signal encoding the desired expression level, and provides the latter with stimuli based on antithetic control logic so as to steer the sensed output towards the desired goal [12], [15], [16].

Our work builds upon the foundation of synthetically engineered microbial consortia, where microbial cooperation, segregation, and division of labor have been leveraged for applications ranging from complex compound production [17] to advanced computational processes [18] (refer to [19]–[21] for a comprehensive review). Despite these advancements, as highlighted in [4], the in vivo implementation of synthetic communities implementing a distributed

feedback control loop for the robust regulation of a desired phenotype to a specific reference value remains unexplored. Prior studies, such as Shou's [22], have established mutualistic interactions between yeast populations for coexistence, and research documented in [23] achieved synchronized oscillations in E. coli strains via an engineered feedback loop. Furthermore, a majority sensing mechanism in a microbial consortium was realized through negative feedback in [24]. While these studies successfully created synthetic microbial consortia with targeted phenotypes, they lack the capability for precise and robust tuning of expression, a critical aspect for advanced synthetic biology applications.

In this paper, we address this fundamental gap in the literature by developing and validating in-vivo a feedback control loop distributed across a bacterial consortium. We demonstrate its effectiveness in regulating a phenotype of interest in the target population even in the presence of variations in the consortium composition. This is achieved by designing two Escherichia coli strains embedding all the modules required to implement the three fundamental functions needed for control, namely computation, sensing and actuation [12]. We show that the designed cellular populations respond to their respective inputs and that the two populations can exchange information through two rationally designed communication channels, implemented using orthogonal quorum sensing signalling molecules. To demonstrate the validity of the proposed strategy, we carry out in-vivo experiments comparing the closed loop configuration, where the controller cells can sense the signalling molecules from the targets, with an open-loop implementation, where they cannot. Our results show that the proposed multicellular control approach can successfully be used to achieve reliable and robust regulation of the expression level of a gene of interest in the targets while guaranteeing robustness to composition imbalances in the consortium, a particularly important property for practical implementations.

Results

A multicellular distributed control architecture

The implementation of a multicellular control architecture requires the rational design of two populations, namely the *controllers* and the *targets* (see Figure 1a). The controllers receive information about the targets' output (y) which is the expression level of some gene of interest

91 therein. This value is compared to that of some reference signal (*ref*) encoding the desired
92 expression level and a control input (u) is then generated via the designed control logic. This
93 signal is transmitted to the targets in order to regulate the level of their output to that encoded
94 by the reference. The communication between controllers and targets is implemented via
95 orthogonal Quorum Sensing molecules, where each cell population produces signalling
96 molecules that can diffuse through the growth environment and into the other population.

97 The control logic, embedded in the controllers, is an antithetic feedback control strategy [3],
98 based on the *in-silico* analysis presented in [12] and derived from the error computation
99 module (comparator) implemented *in-vivo* using molecular titration in [25] and characterized
100 dynamically in [26]. The controller network is a multi-input, single-output device that uses
101 two independent signals to regulate the expression level of its output protein (see Figure 1b).
102 It is constructed around a σ factor [27], which is a protein that recruits RNA polymerase
103 (RNAP) to target promotors by binding to DNA sequences in the -10 and -35 regions of those
104 promoters , and their cognate anti-σ, which blocks the interaction between RNAP and the σ
105 factor by sequestering the σ factor. The production of σ is controlled by IPTG (the reference
106 signal), which induces expression from the promoter *plac-UV5*. The production of anti-σ is
107 regulated by the *plux* promoter, which is activated by the complex formed by LuxR, produced
108 constitutively, and 3-O-C6-HSL, produced by the targets. The output signal of the controllers
109 (3-O-C12-HSL) is produced by the product of the *lasI* gene, which is regulated by the *p20 992*
110 promoter. This promoter, placed upstream of *lasI*, is induced by the presence of the orthogonal
111 σ factor. The σ and anti-σ factors interact by binding and forming a complex that is unable to
112 recruit RNAP to *p20_992*. All proteins are fused to a degradation tag (ssrA tag) [28].

113 The targets can express a green fluorescent protein (GFP), whose expression level we aim to
114 regulate. The *gfp* gene is transcribed together with *luxI*, whose product is responsible for the
115 production of the molecule 3-O-C-6-HSL. This small molecule operates as a proxy of the *gfp*
116 expression levels by diffusing in the growth environment and activating the production of
117 anti-σ in the controllers. The production of LuxI and GFP is regulated by *plas*. This promoter
118 is activated by the complex formed by LasR, which is constitutively expressed, and 3-O-C12-
119 HSL, which is produced by the controller population. In our implementation, LuxI was fused

120 to a degradation tag (ssrA tag) to ensure its fast degradation. All the details of the plasmids
121 and strains used in this work can be found in the *Strains and constructs* section of the Methods.

122 The goal of the design is to make the two engineered populations cooperate to steer and
123 maintain *gfp* expression in the targets at a desired setpoint level, which can be changed by
124 modifying the concentration of IPTG. Specifically, when *gfp* is overexpressed, the excessive
125 production of 3-O-C6-HSL upregulates the production of anti-σ. In turn, a reduction of the
126 free available σ, downregulates the production of LasI and, in turn, of the signalling molecule
127 3-O-C12-HSL. As a consequence, the activity of *pLas* in the targets should be reduced,
128 decreasing GFP expression levels. Similar mechanisms lead to an increase in GFP when GFP
129 falls below the desired level.

130 *Gene expression can be regulated via a multicellular architecture*

131 Prior to mixing the two populations in the consortium, we tested the functional modules
132 embedded in each population using flow cytometry [29]. Details on the machines and the
133 settings used can be found in section *Samples preparation and analysis using flow cytometry* of the
134 Methods.

135 We started by characterizing the response of the controller population to IPTG and 3-O-C6-
136 HSL, which are used in the architecture as a reference signal and a proxy for the targets state,
137 respectively. Note that, to measure the output level of the controllers, we substituted *lasI* with
138 a *gfp* fused with an ssrA tag (see Figure S1). We grew the controllers at 37 ^{o}C for 3h adding
139 different concentrations of IPTG and 3-O-C6-HSL to the growth media to test their response
140 to their inputs. The fluorescence levels of the population was then analysed by Flow
141 Cytometry (for more details see section *Induction protocol* of the Methods). The addition of
142 IPTG promoted *plac-UV5* activity by inhibiting the repression exerted by LacI, thus inducing
143 up to 300 fold increase in the steady state fluorescence when 100 μM IPTG was added to the
144 media (Figure 2a). Conversely, the addition of 3-O-C6-HSL increased the anti-σ level of
145 transcription by activating *plux;* as a consequence, the fluorescence levels consistently
146 decreased, resulting in the inhibition of *gfp* expression levels up to 100 folds when 100 nM 3-
147 O-C6-HSL was added to the growth media (Figure 2a). We used the same procedure to assess
148 the response of the targets to 3-O-C12-HSL; as expected, addition of 10 μM 3-O-C12 in the
149 growth media promoted *plas* activity and a 14 fold increase was detected in average GFP

150 fluorescence (Figure 2b). These assays confirmed that the controllers were correctly
151 responding to changes either in the reference signal or in the output of the targets, and,
152 confirmed that the targets were able to adjust GFP production according to the concentration
153 of 3-O-C12-HSL. For further details on the standard deviation of the response of targets and
154 controllers see Figure S2.

155 We then assayed the ability of the two populations to communicate with each other. To test
156 the ability of the controllers to stimulate the targets in the absence of any feedback from the
157 latter, we implemented an open loop configuration of the consortium where the output
158 sensing module was removed from the controller cells (see Figure 2c, right panel). This made
159 them unable to receive feedback sensing molecules from the targets. We will refer to this
160 population as *open loop controllers*.

161 We mixed the open loop controllers with the targets every hour, grew the consortium at 37 ^{o}C
162 for 6h and analysed the targets fluorescence via flow cytometry (for further details on the
163 experimental protocol see section *Time-course assays* of the methods). This time course,
164 reported in Figure 2d (light blue trajectory), shows that the open loop controllers are able to
165 communicate with the targets, i.e. that the 3-O-C12-HSL is successfully produced by the open
166 loop controllers and sensed by the targets. Indeed, the controllers were able to induce a 15
167 fold increase in the average fluorescence of the targets after 6h. However, over this time period
168 the open loop controllers were not able to stabilize the *gfp* expression levels in the targets
169 confirming that, as expected, they were unable to receive any feedback signal sent from them.
170 We performed similar experiments mixing the controllers with the targets. In closed loop,
171 where controllers possess the module to sense the expression level of the controlled gene in
172 the targets, stabilization of the targets fluorescence was observed after 3h (Figure 2d, yellow
173 trajectory). This confirms that the targets were able to successfully produce 3-O-C6-HSL
174 molecules which were correctly received by the controller population.

175 We then tested the ability of the controllers in the closed loop configuration to regulate *gfp*
176 expression levels in the targets to different values by modulating the concentration of IPTG in
177 the culture medium. Specifically, we grew controllers and targets in coculture at 37 ^{o}C for 6h,
178 both with and without IPTG in the growth medium and then analysed the fluorescence level
179 of the targets using flow cytometry. When the consortium was induced with 50 μM IPTG, the

180 relative increase in fluorescence was approximately 50% (Figure 2e). This increase was
181 surprisingly small compared to the expected increase in the output observed during the
182 preliminary characterisation of the populations. Comparing the 6h timepoint of the closed
183 loop time course without IPTG shown in Figure 2d with the uninduced targets response
184 shown in Figure 2b, we observed that the targets were expressing high levels of fluorescence
185 when mixed with the controllers, even when no IPTG was present in the culture media (Figure
186 S3 shows a comparison of the distribution of fluorescence of the targets in the two scenarios).
187 This suggests that there was an unexpected high basal production of 3-O-C12-HSL, which was
188 not revealed during the initial characterisation of the populations shown in Figure 2a. The
189 inability to reveal the base expression level in the initial characterisation highlights the
190 difference between the expression level needed to detect any GFP signal and the levels of
191 enzyme needed to produce enough signalling molecules to induce the targets.

192 We addressed this problem by reducing the synthesis rate of σ in the absence of IPTG, aiming
193 to increase the range of GFP fluorescence levels we could regulate the targets to. Specifically,
194 we increased the repression efficiency of *plac-UV5* by LacI by adding an extra lac operator
195 upstream of the promoter. This, as shown in [30], reduces the basal expression of the gene
196 controlled by LacI enabling the LacI tetramer to bind two operators simultaneously, thus
197 increasing the apparent affinity of the interaction (see *strains and constructs* section of the
198 methods for more details on the construction of the plasmid). We will henceforth denote the
199 modified controllers/open loop controllers "controllers/open loop controllers 2.0". After
200 adding the extra operator, the steady state fluorescence of the targets in closed loop and open
201 loop was reduced to levels that were lower than the ones reached by uninduced target
202 monocultures after 6h of growth (see Figure 3a,b). This indicated that the addition of the extra
203 operator reduced dramatically the leakiness of the *plac-UV5* promoter. We then repeated the
204 dynamic characterisation of the open and closed loop configurations of the consortium using
205 the new version of both controller populations. In open loop, the open loop controllers 2.0
206 were able to stabilize *gfp* expression levels in the targets after 6h. In addition, by increasing
207 the IPTG concentration in the culture media, we could achieve up to a 10-fold increase in GFP
208 expression levels. However, the regulation was highly variable across the different biological
209 replicates, especially at 0 μM and 3 μM IPTG (see Figure 3a). By closing the feedback loop with
210 the addition of the output sensing module in the controllers, we were able to increase the

211 reliability of the regulation, reducing the standard deviation at the 6h timepoint 5-fold and
212 29-fold, when we used 0 μM and 3 μM IPTG, respectively. In addition, the settling time was
213 comparable to the open loop configuration (approximately 3h), and we were able to induce
214 up to a 5-fold increase when 7 μM IPTG was added to the culture medium (see Figure 3b).

215 We further investigated the tunability of the regulation in both configurations by analysing
216 the steady state response with increasing levels of IPTG (details of the protocol used can be
217 found in the *Titration assays* section of the Methods). Specifically, we mixed the
218 controllers/open loop controllers 2.0 with the targets and grew the consortium for 6h at 37 °C.
219 Figure 3c shows that both consortia were able to regulate the *gfp* gene to different expression
220 levels. Both architectures showed saturation when IPTG $\in [0\ \mu M; 2\ \mu M]$. Above that
221 concentration, increases in IPTG concentrations drove an increase in the targets' fluorescence
222 levels. In addition, both consortia underwent an abrupt increase in the targets' average
223 fluorescence and in its variance when we used IPTG at concentrations above $8\mu M$. Using the
224 remaining data (IPTG $\in [2\ \mu M,\ 8\ \mu M]$), where the response of both systems was mostly linear,
225 we observed some differences in the regulation patterns between the two configurations. The
226 closed loop system showed an almost linear increase in GFP fluorescence, while in open loop
227 we noticed a sharp increase in fluorescence levels between 2μM and 3μM IPTG, followed by
228 much flatter increase in fluorescence when IPTG was present at concentrations above 5 μM.
229 We quantified the linearity of the input-output response of both configurations to IPTG by
230 fitting the data with linear least square estimators and comparing the R^2 values. Using the
231 data where IPTG $\in [2\ \mu M, 8\ \mu M]$, the estimator fitting the closed loop data (yellow dashed line
232 in Figure 3c) predicts almost perfectly the variance coming from the data (R^2 = 0.927). In
233 contrast, the estimator that fits the data obtained using the open loop configuration of the
234 consortium explained just above half of such variance (R^2 = 0.624).

235 In our experiments, we established the effectiveness of a multicellular control architecture in
236 regulating the expression of a desired gene within the target population. Our findings
237 underscore the significant impact of feedback incorporation, leading to a substantial reduction
238 in response variability and enhanced linearity in the input-output relationship of the
239 architecture.

240 *Closed loop control enhances robustness to changes in the consortium composition*

241 A crucial problem when multicellular strategies are deployed in a consortium across multiple
242 cellular populations [31] is that different populations may grow at different rates because of
243 differences in their metabolic loads. This may hinder the ability of the controllers to steer the
244 dynamics of the targets as it might cause fluctuations in the production rate of the sensing (3-
245 O-C6-HSL) and actuation (3-O-C12-HSL) molecules. We therefore analysed the robustness of
246 both the closed loop and the open loop configurations to changes in the consortium
247 composition (see Figure 4).

248 We produced consortia of different compositions by inoculating targets and controllers/open
249 loop controllers 2.0. in different ratios, then measuring the average fluorescence of the targets
250 after 6h (for more detail see section *Consortium composition assay* of the Methods). Figure 4 a-d
251 shows that varying the proportion of controllers2.0. and targets had no detectable effect on
252 the reliability of the regulation of the closed loop configuration, where feedback between the
253 two populations is present. Conversely, in the absence of feedback (in the open-loop
254 configuration), we noted a declining trend in the fluorescence levels of the targets as the
255 percentage of targets increased, especially when 0 μM and 3 μM IPTG concentrations were
256 employed. This trend was not seen when 5 μM and 7 μM IPTG were present in the culture
257 medium. We quantified the difference between the fluorescence of the targets depending on
258 their percentage in the consortium by fitting linear least square estimators to the data (dashed
259 lines in Figure 4 a-d). We then compared the slopes of the lines fitting the open and closed
260 loop datapoints at different IPTG concentrations (see Figure 4 e). Using analysis of covariance
261 and a multiple comparison test, we found that when 0μM and 3μM IPTG were used, the
262 slopes of the linear models fitting the closed and open loop datapoints were statistically
263 different with p-values equal to 0.01527 and 1.13 10^{-6}, respectively. In contrast, when 5μM
264 and 7μM IPTG were present in the culture media, the changes were not significant. This could
265 be attributed to the saturation of the *plas* promoter activity at higher IPTG concentrations,
266 which reduced the sensitivity of the targets to variations in the 3-O-C12-HSL concentration
267 (see Supplementary Figure S4 for more details and section S1 of the Supplementary
268 Information for the details on the protocol used).

269 The analysis was finalized by conducting a statistical comparison of the slopes of the curves
270 fitted to the closed-loop data points across all IPTG concentrations. Employing the same

methodology, we established that there were no significant differences in slopes within the closed-loop system (detailed p-values provided in Table S3). This confirmed the consistent robustness of the multicellular feedback control strategy in maintaining stability, even in the presence of imbalances between the controllers' and targets' populations.

Discussion

Our study presents for the first time the *in-vivo* biological implementation of synthetic feedback controllers within cellular populations, using a multicellular control architecture where, withing a consortium, a specific population of controller cells possesses the ability to sense and regulate targeted phenotypes within another population of cells. This strategic distribution of control functionalities across members of a microbial consortium alleviates the metabolic burden that would otherwise be imposed if all functions were concentrated within a single cell, as noted in prior research [32]. Moreover, this approach enhances the consortium's robustness, enabling it to adapt effectively to changes in its composition.

Following the validation of individual components within our microbial community, we meticulously assessed the architecture's performance and robustness using flow cytometry. Our results unequivocally demonstrate the distributed feedback controller's capability to effectively regulate gene expression within target cells, maintaining the desired levels even in the face of alterations in the consortium's composition. To substantiate the effectiveness of our control architecture, we conducted a comparative analysis between open and closed loop implementations. This examination clearly underscores the pivotal role of feedback mechanisms, revealing that their incorporation significantly enhances both the reliability and robustness of gene regulation within the system.

The development of distributed feedback controllers across microbial communities paves the way for the construction of complex interacting communities, where each population carries out a specific function [21]. Implementation of our distributed consortia within microfluidics/microscopy platforms would allow the realisation of more complex feedback control tasks in space and time [26], [33], [34].

300 Such microbes could be used in applications ranging from the integration of bacteria in the
301 human gut microbiome to treat a class of diseases [35] to engineering the soil microbiome to
302 increase plant growth and health [36], and bacteria-based production of fuels, which presents
303 a promising source for sustainable energy [37].

304 Current theoretical work is aimed at improving the performance and robustness of the
305 proposed design by expanding the consortium to include additional controller populations,
306 adding, for example, populations able to implement proportional or derivative control actions
307 in order to achieve a multicellular implementation of biomolecular PID controllers recently
308 proposed in [7], [15], [38].

309 **Methods**

310 *Strains and constructs*

311 *Escherichia coli* strain TOP10 was used for all the cloning manipulations of this work.
312 *Escherichia coli* strain MG1655 λ-, rph-1 [39] was used for all the assays in this work and
313 transformed with the plasmids constituting either the controllers or the targets. For all the
314 sequences of the primers and the synthesised genes used in this study see Table S1, Table S2.
315 In addition, all the maps of the plasmids are reported In Figure S5.

316 The controllers contain three plasmids: pVRa20_992_BS2 (medium copy number),
317 pVRc20_992_BS1 (medium copy number) and pVRb_LasI (low copy number). The genes
318 constituting the essential core of the computation module (σ, anti-σ and lasI) are ssrA tagged
319 (AANDENYALAA) to ensure fast dynamics of expression and degradation [28].

320 pVRb_lasI encodes the *lasI* gene, under the control of the *p_20992* promoter, and was built in
321 [15], together with pVRb_ssrA, where the lasI gene was swapped with a superfolder *gfp*.
322 pVRb_lasI was present in the controllers in each of the assays where they were mixed with
323 the targets, whereas pVRb_ssra was present in the controllers for their input output
324 characterisation.

325 Vector backbones for pVRa20_992_BS2 and pVRc20_992_BS1 were derived from plasmids
326 pVRa20_992 and pVRc20_992 [27]. pVRa20_992_BS2 produces a σ factor under the control of
327 a promoter that responds to IPTG.. To construct this plasmid, first the pVRa20_992_BS1
328 plasmid was obtained by standard restriction digestion and ligation procedure, by amplifying

329 the σ gene from the pLusB plasmid [25] with primers Sigma_plus_tag_F and
330 Sigma_plus_tag_R and cloning the PCR product in the pVRa_20_992 plasmid after
331 NcoI/BamHI digestion. Then, the *plac* promoter was substituted with *plac-UV5* to obtain the
332 pVRa20_992_BS2 plasmid. The construct was built by standard restriction digestion and
333 ligation procedure, by amplifying *plac-UV5* from the pVRa_placASb_Flag plasmid [25] with
334 primers PlacUV5_F and PlacUV5_R and cloning the PCR product in pVRa_20_992_BS1
335 plasmid after XbaI digestion. Finally, we modified pVRa_20_992_BS2 by introducing a second
336 lac operator upstream of *plac_UV5*. This construct, denoted as PVRa_20_992_DS, was
337 constructed by Gibson assembly after PCR amplification of pVRa20_992_BS2 using primers
338 Back_extralac_for and Back_extralac_rev, and of the pVRbLacO1O1Del from [40] using the
339 Ins_extralac_for and Ins_extralac_rev primers. pVRc20_992_BS1 produces the anti-σ factor
340 under the induction of 3-O-C6-HSL. The plasmid was constructed by standard restriction
341 digestion and ligation procedure, by amplifying anti-σ from pVRa_placASb_Flag [25] with
342 primers Anti_Sigma_plus_tag_F and Anti_Sigma_plus_tag_R and cloning the PCR product
343 in pVRc_20_992 plasmid after BamHI/PstI digestion. Finally, the controllers expressing a Red
344 Fluorescent Protein were implemented by substituting the pVRb_lasI plasmid with the
345 pVRb_lasI_RFP plasmid. pVRb_lasI_RFP was assembled using standard restriction digestion
346 and ligation procedure, by amplifying a synthetically generated RFP with primers
347 RFP_Afe_for and RFP_Nde_rev and cloning the PCR product in the pVRb_lasI plasmid after
348 AfeI/NdeI digestion.

349 The targets hosted p_Las_Lux_GFP_3.0, a plasmid that embeds the 3-O-C12-HSL inducible
350 promoter *plas,* driving the expression of a mut3 green fluorescent protein and of the luxI gene
351 (fused with and ssrA tag). This plasmid was assembled by Gibson assembly after PCR
352 amplification of the las_composite_device plasmid from [41] with
353 p_Las_Lux_GFP_3_0_fwd_20 and p_Las_Lux_GFP_3_0_rev_20 primers, and of the luxI from
354 pTeLu_GFP constructed in [25] with the luxI_fwd and luxI_rev primers.

355 *Chemicals*

356 For all experiments, kanamycin (50 μg/mL), ampicillin (100 μg/mL) and chloramphenicol (25
357 μg/mL) were added to the growth media, depending on the bacteria selective resistance. These
358 antibiotics were supplied by Sigma-Aldrich. pVRa_20992_BS2 and pVRa_20_992_DS have an

359 Ampicillin resistant gene, pVRb_lasI, pVRB_lasI_RFP and pVRb_ssrA have a gene conferring
360 Kanamycin resistantce, and pVRc_20_992_BS1 and p_Las_Lux_GFP_3.0 have a gene
361 guaranteeing Chroranmphenicol resistance. When multiple populations were mixed, the
362 antibiotics to which both populations were resistant were used. If no resistance was in
363 common, no antibiotic was used.

364 3-O-C6-HSL (N-(B-Ketocaproyl)-L-Homoserine Lactone from Sigma-Aldrich, cat # K3007)
365 and 3-O-C12-HSL (N-(3-Oxododecanoyl)-L-homoserine lactone from Sigma-Aldrich, cat #
366 O9139) were dissolved in DMSO, filter-sterilized and added to the LB growth medium at the
367 indicated concentrations. IPTG (Isopropyl β-D-1-thiogalactopyranoside, supplied by Sigma-
368 Aldrich, cat # I5502) was dissolved in water, filter-sterilized and added to LB medium at the
369 indicated concentrations.

370 *Samples preparation and analysis using flow cytometry*

371 Each sample (0.5 mL volume) was resuspended in 1xPBS and diluted to achieve a final OD_{600}
372 for the culture of 0.05. Data were acquired using either BD LSRFortessa X-20 or Acea Novocyte
373 flow cytometer. The results analysed using FlowJo.

374 The events recorded by a flow cytometer were first gated in the forward scatter (FSC-H, proxy
375 of cellular size), side scatter (SSC-H, proxy of cellular complexity) plane. Here, the events were
376 divided in three subpopulations: healthy cells where size and complexity were in
377 physiological ranges [42], stressed cells where the bacteria had increased size and complexity
378 due to filamentation, and cellular debris corresponding to events with high size with respect
379 to their complexity (Figure S6 a). Subsequently, healthy cells were gated in the SSC-H, SSC-A
380 plane to select for single cells. Cells with comparable signals in the two channels were selected
381 as single cells, whereas events with much larger SSC-A were classified as cellular
382 conglomerates and excluded from the analysis (Figure S6b). Finally, single cells were gated
383 using the FITC-H (Novocyte machine)/FITC-A (Fortessa machine) (490 nm excitation, 530/30
384 nm emission) channel to discriminate targets and controllers based on their fluorescence
385 levels. Specifically, cells with low FITC-H signal were classified as controllers and cells having
386 high FITC-H fluorescence were selected to be targets (Figure S6c). Alternatively, when
387 controllers constitutively expressed RFP, events with a high signal in the PE-CF594 (560 nm

388 excitation, 610/20 nm emission filter, Red) channel were distinguished as controllers while
389 cells with low signal were designated as targets.

390 *Induction protocol*

391 Cells were cultured in 10 mL LB broth in 50 mL Falcon tubes. 20μL of overnight cultures were
392 added to the media, which was supplemented with the inducer(s) at the specified
393 concentration. The culture was then incubated at 37 ^{o}C, shaking at 250rpm for 3h. Then, the
394 samples were prepared and analysed by flow cytometry. This protocol was used to obtain
395 Figures 2 a,b.

396 *Time-course assays*

397 35 μL of overnight cultures of controllers and 140 μL of overnight cultures of targets were
398 separately diluted each in 35 mL LB added to a 250mL sterile flask. Each culture was
399 supplemented with the specified concentration of IPTG. Both cultures were incubated at 37
400 ^{o}C, shaking at 250rpm for 6h. Each hour, 5 mL of both cultures were mixed in sterile 50 mL
401 tubes, which were then incubated alongside the single strain cultures. After 6h, 0.5 mL of all
402 mixed cultures were sampled and analysed via flow cytometry. Note that the hours in Figure
403 2c and Figure 3a,b refer to the time targets and controllers have been mixed for. Figure 2c
404 Figure 3a,b were obtained using this protocol.

405 *Titration assay*

406 For each condition, 8μL of overnight culture of targets and 2μL of overnight culture of
407 controllers were mixed in 10 mL LB broth in 50 mL Falcon tubes. Each culture was
408 supplemented with IPTG at the specified concentration. The cultures were then incubated at
409 37 ^{o}C, shaking at 250rpm for 6h. Then, the samples were prepared and analysed by flow
410 cytometry. This protocol was used to obtain Figure 3 c.

411 *Consortium composition assay*

412 Overnight cultures of targets and controllers were diluted in 10 mL LB using different
413 targets:controllers ratios. Specifically, 15:1, 8:1, 4:1, 2:1, 1:1 ratios were created by adding 10μL
414 of controllers and 150 μL, 80 μL, 40 μL, 20 μL, 10 μL of targets, respectively. All cultures were

415 incubated at 37 °C shaking at 250rpm for 6h. Then, 0.5 mL of each culture was sampled and
416 analysed by flow cytometry. This protocol was used in Figure 2d, Figure 4a-d.

417

418 **Data availability**

419 The authors declare that the data supporting the findings of this study are available within
420 the paper and its Supplementary Information files or from the corresponding author on
421 reasonable request. The source data underlying all figures in the main text and supplementary
422 information are provided as a Source Data file.

423

424 **Acknowledgements**

425 The authors wish to acknowledge Gwen Brouwer and Abigail Smith for their support with
426 the cloning of the constructs needed for this work. Also, the authors also wish to
427 acknowledge the FACS facility hosted at the University of Bristol for their support with the
428 use of the Flow Cytometers. M.d.B., L.M. wish to acknowledge support from the European
429 Project FET-OPEN Cosy-Bio (Grant Agreement number 766840). M.d.B. also wishes to
430 acknowledge support from the PNRR and PNC projects of the Italian Government. L.M.
431 acknowledges funding from the Engineering and Physical Sciences Research Council
432 (EPSRC, Fellowship EP/S01876X/1) and the Biotechnology and Biological Sciences Research
433 Council (BrisEngBio grant, BB/W013959/1). Finally, L.M., N.J.S., C.G. and M.d.B. wish to
434 acknowledge support form BrisSynBio, a BBSRC/EPSRC Synthetic Biology Research Centre
435 (BB/L01386X/1).

436

437 **Author Contributions**

438

439 M.d.B, L.M., N.J.S. and C.G. designed the research; D.S. designed the experiments; D.S. and
440 B.Scarried out the experiments; D.S. with support from M.d.B., L.M., N.J.S. and C.G. analyzed
441 the data; D.S. and M.d.B. wrote the manuscript with inputs from L.M., N.J.S. and C.G.

Competing Interests

The authors declare no competing interests.

References

[1] D. Del Vecchio, Y. Qian, R. M. Murray, and E. D. Sontag, 'Future systems and control research in synthetic biology', *Annual Reviews in Control*, vol. 45, pp. 5–17, 2018, doi: 10.1016/j.arcontrol.2018.04.007.

[2] D. E. Cameron, C. J. Bashor, and J. J. Collins, 'A brief history of synthetic biology', *Nat Rev Microbiol*, vol. 12, no. 5, pp. 381–390, May 2014, doi: 10.1038/nrmicro3239.

[3] M. Filo, C.-H. Chang, and M. Khammash, 'Biomolecular feedback controllers: from theory to applications', *Current Opinion in Biotechnology*, vol. 79, p. 102882, Feb. 2023, doi: 10.1016/j.copbio.2022.102882.

[4] M. H. Khammash, 'Cybergenetics: Theory and Applications of Genetic Control Systems', *Proc. IEEE*, vol. 110, no. 5, pp. 631–658, May 2022, doi: 10.1109/JPROC.2022.3170599.

[5] I. Ruolo, S. Napolitano, D. Salzano, M. Di Bernardo, and D. Di Bernardo, 'Control engineering meets synthetic biology: Foundations and applications', *Current Opinion in Systems Biology*, vol. 28, p. 100397, Dec. 2021, doi: 10.1016/j.coisb.2021.100397.

[6] C. Briat, A. Gupta, and M. Khammash, 'Antithetic Integral Feedback Ensures Robust Perfect Adaptation in Noisy Biomolecular Networks', *Cell Systems*, vol. 2, no. 1, pp. 15–26, Jan. 2016, doi: 10.1016/j.cels.2016.01.004.

[7] M. Filo, S. Kumar, and M. Khammash, 'A hierarchy of biomolecular proportional-integral-derivative feedback controllers for robust perfect adaptation and dynamic performance', *Nat Commun*, vol. 13, no. 1, p. 2119, Apr. 2022, doi: 10.1038/s41467-022-29640-7.

[8] C. Briat, A. Gupta, and M. Khammash, 'Antithetic proportional-integral feedback for reduced variance and improved control performance of stochastic reaction networks', *J. R. Soc. Interface.*, vol. 15, no. 143, p. 20180079, Jun. 2018, doi: 10.1098/rsif.2018.0079.

[9] M. Chevalier, M. Gómez-Schiavon, A. H. Ng, and H. El-Samad, 'Design and Analysis of a Proportional-Integral-Derivative Controller with Biological Molecules', *Cell Systems*, vol. 9, no. 4, pp. 338-353.e10, Oct. 2019, doi: 10.1016/j.cels.2019.08.010.

[10] S. K. Aoki, G. Lillacci, A. Gupta, A. Baumschlager, D. Schweingruber, and M. Khammash, 'A universal biomolecular integral feedback controller for robust perfect adaptation', *Nature*, vol. 570, no. 7762, pp. 533–537, Jun. 2019, doi: 10.1038/s41586-019-1321-1.

[11] T. Frei, C.-H. Chang, M. Filo, A. Arampatzis, and M. Khammash, 'A genetic mammalian proportional–integral feedback control circuit for robust and precise gene

regulation', *Proc. Natl. Acad. Sci. U.S.A.*, vol. 119, no. 24, p. e2122132119, Jun. 2022, doi: 10.1073/pnas.2122132119.

[12] G. Fiore *et al.*, '*In-Silico* Analysis and Implementation of a Multicellular Feedback Control Strategy in a Synthetic Bacterial Consortium', *ACS Synth. Biol.*, vol. 6, no. 3, pp. 507–517, Mar. 2017, doi: 10.1021/acssynbio.6b00220.

[13] F. Bullo, J. Cortés, and S. Martínez, *Distributed Control of Robotic Networks: A Mathematical Approach to Motion Coordination Algorithms*. Princeton University Press, 2009. doi: 10.1515/9781400831470.

[14] G. Antonelli, 'Interconnected dynamic systems: An overview on distributed control', *IEEE Control Syst.*, vol. 33, no. 1, pp. 76–88, Feb. 2013, doi: 10.1109/MCS.2012.2225929.

[15] V. Martinelli, D. Salzano, D. Fiore, and M. Di Bernardo, 'Multicellular PI Control for Gene Regulation in Microbial Consortia', IEEE Control Syst. Lett., vol. 6, pp. 3373–3378, 2022, doi: 10.1109/LCSYS.2022.3184922.

[16] D. Fiore, D. Salzano, E. Cristobal-Coppulo, J. M. Olm, and M. Di Bernardo, 'Multicellular Feedback Control of a Genetic Toggle-Switch in Microbial Consortia', *IEEE Control Syst. Lett.*, vol. 5, no. 1, pp. 151–156, Jan. 2021, doi: 10.1109/LCSYS.2020.3000954.

[17] S. Sosa-Carrillo, H. Galez, S. Napolitano, F. Bertaux, and G. Batt, 'Maximizing protein production by keeping cells at optimal secretory stress levels using real-time control approaches', *Nat Commun*, vol. 14, no. 1, p. 3028, May 2023, doi: 10.1038/s41467-023-38807-9.

[18] X. Li, L. Rizik, V. Kravchik, M. Khoury, N. Korin, and R. Daniel, 'Synthetic neural-like computing in microbial consortia for pattern recognition', *Nat Commun*, vol. 12, no. 1, p. 3139, May 2021, doi: 10.1038/s41467-021-23336-0.

[19] N. S. McCarty and R. Ledesma-Amaro, 'Synthetic Biology Tools to Engineer Microbial Communities for Biotechnology', *Trends in Biotechnology*, vol. 37, no. 2, pp. 181–197, Feb. 2019, doi: 10.1016/j.tibtech.2018.11.002.

[20] H. Song, M.-Z. Ding, X.-Q. Jia, Q. Ma, and Y.-J. Yuan, 'Synthetic microbial consortia: from systematic analysis to construction and applications', *Chem. Soc. Rev.*, vol. 43, no. 20, pp. 6954–6981, Jul. 2014, doi: 10.1039/C4CS00114A.

[21] N. E. Grandel, K. Reyes Gamas, and M. R. Bennett, 'Control of synthetic microbial consortia in time, space, and composition', *Trends in Microbiology*, vol. 29, no. 12, pp. 1095–1105, Dec. 2021, doi: 10.1016/j.tim.2021.04.001.

[22] W. Shou, S. Ram, and J. M. G. Vilar, 'Synthetic cooperation in engineered yeast populations', *Proc. Natl. Acad. Sci. U.S.A.*, vol. 104, no. 6, pp. 1877–1882, Feb. 2007, doi: 10.1073/pnas.0610575104.

[23] Y. Chen, J. K. Kim, A. J. Hirning, K. Josić, and M. R. Bennett, 'Emergent genetic oscillations in a synthetic microbial consortium', *Science*, vol. 349, no. 6251, pp. 986–989, Aug. 2015, doi: 10.1126/science.aaa3794.

[24] R. N. Alnahhas *et al.*, 'Majority sensing in synthetic microbial consortia', *Nat Commun*, vol. 11, no. 1, p. 3659, Jul. 2020, doi: 10.1038/s41467-020-17475-z.

[25] F. Annunziata *et al.*, 'An Orthogonal Multi-input Integration System to Control Gene Expression in *Escherichia coli*', *ACS Synth. Biol.*, vol. 6, no. 10, pp. 1816–1824, Oct. 2017, doi: 10.1021/acssynbio.7b00109.

[26] B. Shannon *et al.*, '*In Vivo* Feedback Control of an Antithetic Molecular-Titration Motif in *Escherichia coli* Using Microfluidics', *ACS Synth. Biol.*, vol. 9, no. 10, pp. 2617–2624, Oct. 2020, doi: 10.1021/acssynbio.0c00105.

[27] V. A. Rhodius *et al.*, 'Design of orthogonal genetic switches based on a crosstalk map of σs, anti-σs, and promoters', *Molecular Systems Biology*, vol. 9, no. 1, p. 702, Jan. 2013, doi: 10.1038/msb.2013.58.

[28] K. E. McGinness, T. A. Baker, and R. T. Sauer, 'Engineering Controllable Protein Degradation', *Molecular Cell*, vol. 22, no. 5, pp. 701–707, Jun. 2006, doi: 10.1016/j.molcel.2006.04.027.

[29] K. M. McKinnon, 'Flow Cytometry: An Overview', *CP in Immunology*, vol. 120, no. 1, Jan. 2018, doi: 10.1002/cpim.40.

[30] S. Oehler, E. R. Eismann, H. Krämer, and B. Müller-Hill, 'The three operators of the lac operon cooperate in repression.', *The EMBO Journal*, vol. 9, no. 4, pp. 973–979, Apr. 1990, doi: 10.1002/j.1460-2075.1990.tb08199.x.

[31] D. Salzano, D. Fiore, and M. Di Bernardo, 'Ratiometric control of cell phenotypes in monostrain microbial consortia', *J. R. Soc. Interface.*, vol. 19, no. 192, p. 20220335, Jul. 2022, doi: 10.1098/rsif.2022.0335.

[32] S. Jayanthi, K. S. Nilgiriwala, and D. Del Vecchio, 'Retroactivity Controls the Temporal Dynamics of Gene Transcription', *ACS Synth. Biol.*, vol. 2, no. 8, pp. 431–441, Aug. 2013, doi: 10.1021/sb300098w.

[33] I. De Cesare, D. Salzano, M. Di Bernardo, L. Renson, and L. Marucci, 'Control-Based Continuation: A New Approach to Prototype Synthetic Gene Networks', *ACS Synth. Biol.*, vol. 11, no. 7, pp. 2300–2313, Jul. 2022, doi: 10.1021/acssynbio.1c00632.

[34] E. Pedone *et al.*, 'Cheetah: A Computational Toolkit for Cybergenetic Control', *ACS Synth. Biol.*, vol. 10, no. 5, pp. 979–989, May 2021, doi: 10.1021/acssynbio.0c00463.

[35] I. Y. Hwang and M. W. Chang, 'Engineering commensal bacteria to rewire host–microbiome interactions', *Current Opinion in Biotechnology*, vol. 62, pp. 116–122, Apr. 2020, doi: 10.1016/j.copbio.2019.09.007.

[36] Y. Arif, P. Singh, H. Siddiqui, A. Bajguz, and S. Hayat, 'Salinity induced physiological and biochemical changes in plants: An omic approach towards salt stress tolerance', *Plant Physiology and Biochemistry*, vol. 156, pp. 64–77, Nov. 2020, doi: 10.1016/j.plaphy.2020.08.042.

[37] T. S. Bayer, D. M. Widmaier, K. Temme, E. A. Mirsky, D. V. Santi, and C. A. Voigt, 'Synthesis of Methyl Halides from Biomass Using Engineered Microbes', *J. Am. Chem. Soc.*, vol. 131, no. 18, pp. 6508–6515, May 2009, doi: 10.1021/ja809461u.

[38] V. Martinelli, D. Salzano, D. Fiore, and M. Di Bernardo, 'Multicellular PD Control in Microbial Consortia', *IEEE Control Syst. Lett.*, vol. 7, pp. 2641–2646, 2023, doi: 10.1109/LCSYS.2023.3287136.

[39] M. S. Guyer, R. R. Reed, J. A. Steitz, and K. B. Low, 'Identification of a sex-factor-affinity site in E. coli as gamma delta', *Cold Spring Harbor symposia on quantitative biology*, vol. 45, pp. 135--140, 1981.

[40] A. J. Smith, F. Thomas, D. Shoemark, D. N. Woolfson, and N. J. Savery, 'Guiding Biomolecular Interactions in Cells Using *de Novo* Protein–Protein Interfaces', *ACS Synth. Biol.*, vol. 8, no. 6, pp. 1284–1293, Jun. 2019, doi: 10.1021/acssynbio.8b00501.

[41] N. Kylilis, Z. A. Tuza, G.-B. Stan, and K. M. Polizzi, 'Tools for engineering coordinated system behaviour in synthetic microbial consortia', *Nat Commun*, vol. 9, no. 1, p. 2677, Jul. 2018, doi: 10.1038/s41467-018-05046-2.

[42] D. F. Ackerley, Y. Barak, S. V. Lynch, J. Curtin, and A. Matin, 'Effect of Chromate Stress on *Escherichia coli* K-12', *J Bacteriol*, vol. 188, no. 9, pp. 3371–3381, May 2006, doi: 10.1128/JB.188.9.3371-3381.2006.

575

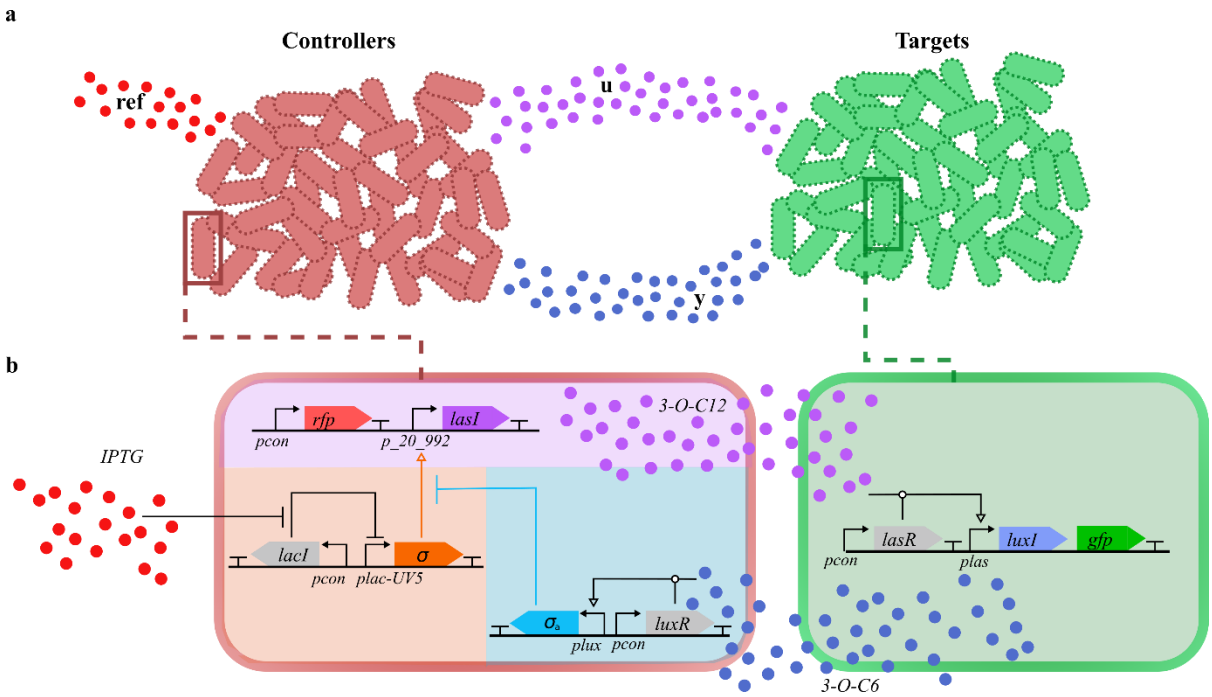

576

577 Figure 1 **Multicellular control schematic. A** Microbial consortium implementing a
578 multicellular control architecture. The two populations, i.e. controllers and targets, share
579 information using orthogonal quorum sensing channels (**u** and **y**), playing the role of the
580 control input and the output of the process, respectively. In addition, the controllers sense
581 the external stimulus labeled as **ref,** used to set up the reference of the feedback loop. **b.**
582 Biological implementation of the multicellular control architecture. The Synthetic Biology
583 Open Language (SBOL) notation is used to denote promoters, genes, promotion/inhibition
584 relationships and quorum sensing molecules. The shaded areas identify different functional
585 modules within each population.

586

587

588

589

590

591

592

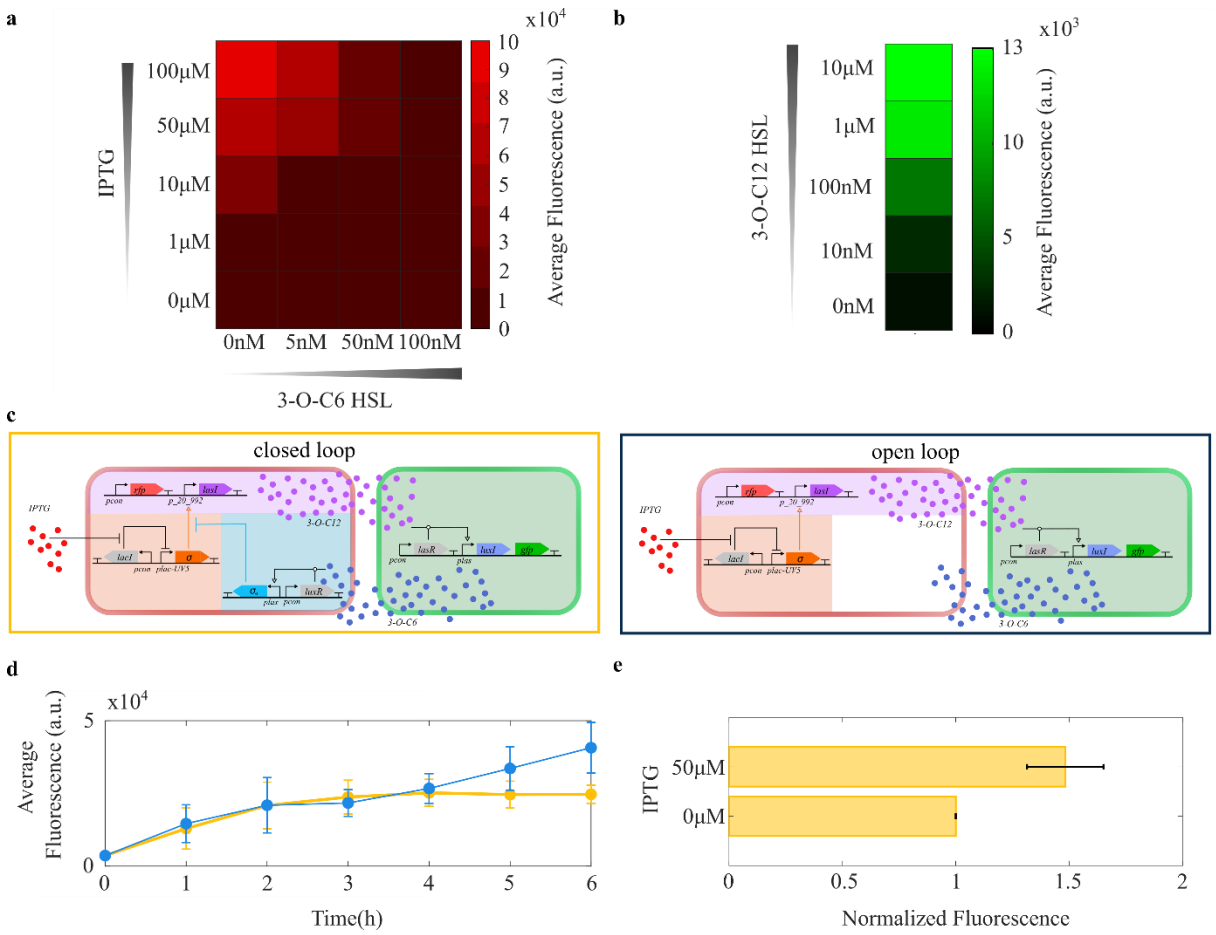

Figure 2 **Characterization of the controllers and targets cell populations. a:** Average fluorescence of the controller population induced using different concentrations of 3-O-C6-HSL and IPTG. The data were collected after 3h from the initial inoculation. **b:** Average fluorescence levels of the target population induced using 3-O-C12-HSL. The data were collected after 3h from the initial inoculation. **c:** Schematic representation of the closed loop (left) and the open loop (right) configurations. **d:** Average fluorescence of the targets over a 6h time course in open (blue) and closed (yellow) loop. The solid dots and vertical bars represent the average and standard deviation over n=3 biological replicates, respectively. **e:** Normalized average fluorescence of the targets mixed with the controllers in closed loop when 0 μM and 50 μM IPTG were present in the growth media. The data were collected 6h after the initial inoculation. The fluorescence was normalized to the average fluorescence reached when no IPTG was added in the media. All data are averaged over n=3 biological replicates.

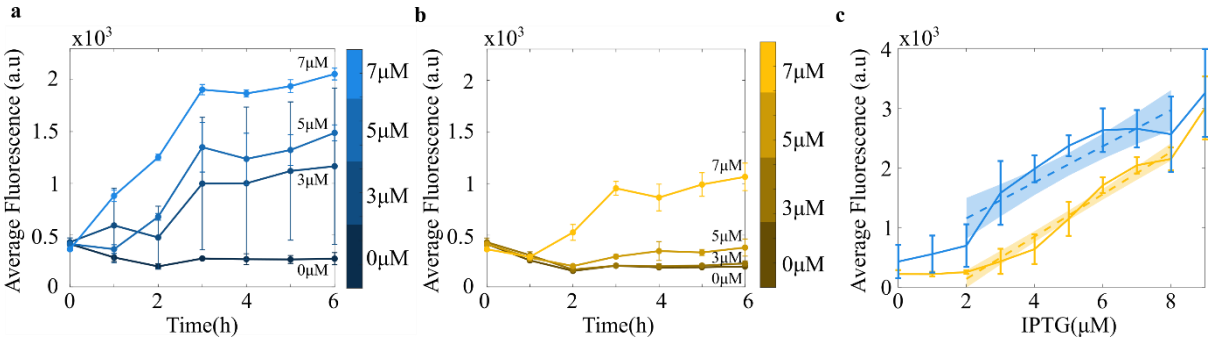

Figure 3 **Regulation of the targets fluorescence using open and closed loop control using controllers2.0/open loop controllers 2.0. a.** Average fluorescence of the targets over a 6h time course, using an open loop control architecture. The solid dots represent the average and the vertical bars the standard deviation of the data over n=3 biological replicates. Each trajectory is color coded and labelled with respect to the concentration of IPTG used in the experiment. **b.** Average fluorescence of the targets over a 6h time course, using a closed loop control architecture. The solid dots represent the average and the vertical bars the standard deviation of the data over n=3 biological replicates. Each trajectory is color coded and labelled with respect to the concentration of IPTG used in the experiment. **c.** Average steady state fluorescence of the targets over different IPTG concentrations. The blue (open loop) and yellow (closed loop) vertical bars are centered on the average values and their amplitude represented the standard deviation of the data over n=3 biological replicates. The dashed lines represent the linear interpolation of the data obtained with IPTG concentrations in the range $[2\ \mu M,\ 8\ \mu M]$. The shaded areas represent the confidence intervals of the linear model prediction. All steady states are collected after 6h from the initial inoculation.

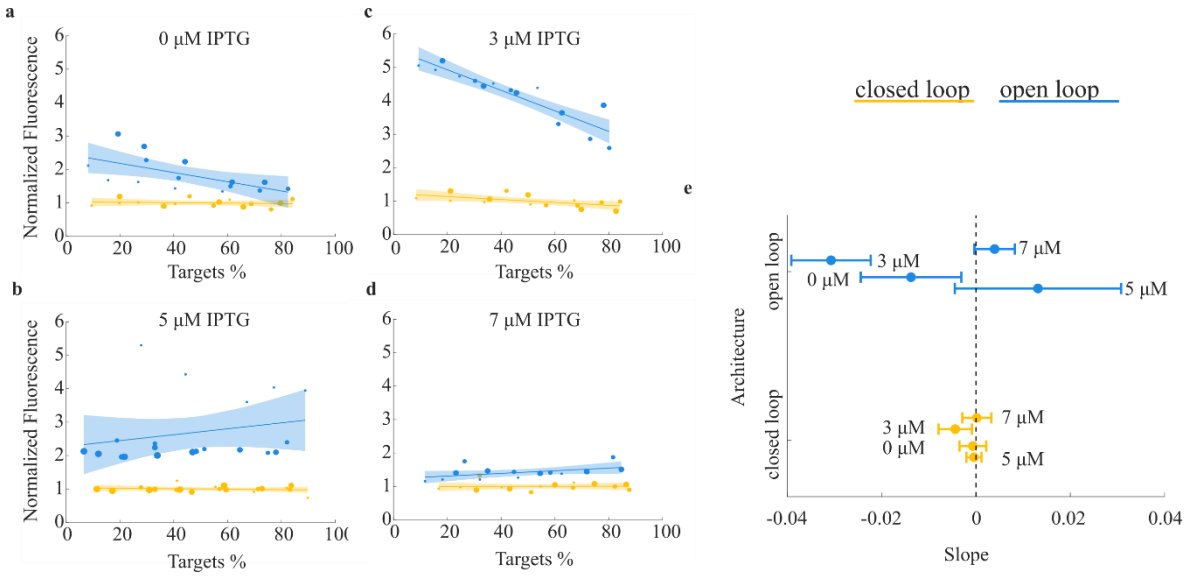

Figure 4 **Closed loop control robustness to changes consortium composition. a-d.** Normalized average fluorescence in open (blue) and closed (yellow) loop across different consortium compositions using controllers 2.0. /open loop controllers 2.0. . The solid dots are the data collected over n=3 biological replicates. Dots of the same size belong to the same replicate. The data were fitted with a first order polynomial. The fitting and its confidence intervals are represented with the solid lines and the shaded areas, respectively. For each replicate, the data are normalized to the average fluorescence reached in closed loop across all compositions. **e.** Comparison of the estimates of the slopes of the linear fittings of data in panels **a-d** when a closed (yellow) or open (blue) loop architecture was used. The solid dots represent the slope estimates and the horizontal bars the 90% confidence interval on the estimates.